Anisotropic magnetic properties of the triangular plane lattice material TmMgGaO$_4$

F. Alex Cevallos, Karoline Stolze, Tai Kong, and R.J. Cava

Department of Chemistry, Princeton University, Princeton NJ 08544 USA

*Corresponding authors: fac2@princeton.edu (F. Alex Cevallos), rcava@princeton.edu (R.J. Cava)

Abstract

The crystal growth, structure, and basic magnetic properties of TmMgGaO$_4$ are reported. The Tm ions are located in a planar triangular lattice consisting of distorted TmO$_6$ octahedra, while the Mg and Ga atoms randomly occupy intermediary bilayers of M-O triangular bipyramids. The Tm ions are positionally disordered. The material displays an antiferromagnetic Curie Weiss theta of ~ -20 -25 K, with no clear ordering visible in the magnetic susceptibility down to 1.8 K; the structure and magnetic properties suggest that ordering of the magnetic moments is frustrated by both structural disorder and the triangular magnetic motif. Single crystal magnetization measurements indicate that the magnetic properties are highly anisotropic, with large moments measured perpendicular to the triangular planes. At 2 K, a broad step-like feature is seen in the field-dependent magnetization perpendicular to the plane on applied field near 2 Tesla.

Introduction

Geometrically frustrated magnetism has been an actively studied property of materials since at least the 1970s[1-2]. In a geometrically frustrated system, the geometry of the crystal lattice inhibits the long-range ordering of the magnetic moments; the simplest examples are systems with antiferromagnetic nearest neighbor interactions on a triangular lattice. As there is no simple way to order the spins in such a system, the magnetic ordering transition will typically be below the Weiss temperature. Geometrically frustrated systems can be used to study a variety of unusual ground state conditions that are difficult to achieve in more conventional materials[1-7]. The influence of structural disorder, especially in geometrically frustrated rare-earth based systems, is expected to be significant[4].

The $YbFe_2O_4$ structure type has been observed to demonstrate a wide variety of electronic and magnetic properties, including geometric magnetic frustration, spin-glass behavior[7-11], charge density waves[12-13], and ferroelectricity[14-16]. This structure crystallizes in the *R-3m* space group, and is defined by triangular planes of metal-oxygen octahedra separated by a bilayer of metal-oxygen triangular bipyramids[17]. Recently, the $YbFe_2O_4$-type compound $YbMgGaO_4$ has drawn interest as a potential candidate for exhibiting quantum spin liquid (QSL) behavior[18-21]. $YbMgGaO_4$ places the magnetic Yb^{3+} ions on the triangular planes, with non-magnetic Mg^{2+} and Ga^{3+} ions randomly mixed in the triangular bipyramidal sites (but with no mixing between magnetic and nonmagnetic ions). The Mg-Ga mixing, off the magnetic plane, causes a considerable variation in local magnetic interactions that is reflected in the compound's properties[20, 22-23]. Here we report the structure and elementary magnetic properties of the isostructural and closely related compound $TmMgGaO_4$, in which similarly complex magnetic behavior is possible. Our results suggest that further, more detailed study may be of future interest.

Experimental

Synthesis

Polycrystalline samples of $TmMgGaO_4$ were synthesized via solid state reaction. Stoichiometric quantities of Tm_2O_3 (99.99%, Alfa Aesar), Ga_2O_3 (99.999%, Alfa Aesar) and MgO

(99.95%, Alfa Aesar) were ground with an agate mortar and pestle. Pellets of the starting composition were heated in ceramic crucibles in air at 1450°C for four days, with intermediate grinding. A small amount of impurity, believed to be $Tm_3Ga_5O_{12}$, was observed in some samples and attributed to an insufficient starting quantity of MgO due to partial hydration of the starting material. The addition of MgO to the impure sample at the 5% level, followed by reheating at 1450°C for 24 hours resulted in the reduction or elimination of this impurity in all cases.

Single crystals in the mm size range were grown by the floating zone method. Single phase polycrystalline powder was loaded into rubber tubes and hydrostatically compressed at 40 MPa, resulting in polycrystalline rods typically measuring 6 mm in diameter and 5-8 cm in length. The rods were then sintered at 1450°C for 3 hours in air before being transferred to a four-mirror optical floating zone (FZ) furnace (Crystal Systems, Inc. Model No. FZ-T-10000-HVP-II-P) with 4 x 1000 W lamps. The rods were then further sintered in the FZ furnace at 65.0% output power, rotating at 15 RPM, with a rate of travel of 1.5 mm/hr. Crystal growth from the feed rods was performed at 68.0% output power, with rods rotating in opposite directions at 20 RPM and an upwards travel rate of 0.5 mm/hr. Growth of faceted millimeter-scale crystals of $TmMgGaO_4$ was observed within a few mm of growth initiation, but large single crystals were not obtained for growths up to 5 cm in length, even when using previous growths as a seed.

Characterization

Room-temperature powder X-ray diffraction (PXRD) measurements were performed with a Bruker D8 Advance Eco diffractometer with Cu $K\alpha$ radiation ($\lambda = 1.5418$ Å) and a LynxEye-XE detector. Phase identification was performed using the Bruker EVA program. Powder Rietveld refinements were performed using Fullprof Suite. Magnetic measurements were taken using a Quantum Design Physical Property Measurement System (PPMS) Dynacool with a vibrating sample mount. DC magnetic susceptibility, defined as the measured magnetization M divided by the applied magnetic field, was measured between 1.8 K and 300 K in an applied field of 1000 Oe, and the resulting values

were divided by the number of moles of Tm^{3+} present to obtain the magnetization values per formula unit. Field-dependent magnetization was measured at 2 K. Powder samples for magnetic characterization were obtained by grinding small single crystals. Anisotropic magnetization measurements were taken on a 1 x 0.2 mm plate-like single crystal (large face perpendicular to the c-axis), either mounted on a silica sample holder with GE varnish or placed in a plastic sample holder, and oriented along the axis of study.

Results and Discussion

Structure

TmMgGaO$_4$, as has been previously reported[24], is isostructural to YbFe$_2$O$_4$, and therefore to a large family of related isostructural $Ln^{+2}M^{2+}M^{3+}O_4$ compounds[8, 25-26]. In agreement with previous reports, our colorless, transparent TmMgGaO$_4$ crystallizes in the space group *R-3m* (166), with lattice parameters of a = 3.4195(3) Å and c = 25.1231(1) Å. The structure is composed of triangular layers of distorted TmO$_6$ octahedra, separated by bilayers of mixed occupancy Mg- and Ga-O triangular bipyramids (Figure 2). The Tm atoms sit displaced, slightly off the ideal [0 0 0] position along *c*, with z = 0.0078(2). This displacement has been observed in other materials in this family and is attributed to the random distribution of non-lanthanide metals in the neighboring bilayers[8]. As the Tm atom can only occupy one of the resulting displaced sites, they must have 1/2 occupancy as the sites are too close together to be simultaneously occupied. Although the lattice parameters and overall structure are in good agreement with previously published results[24-25], the disordered slightly off-ideal location of the Tm^{3+} ion was not noted in the only previous study reporting refined atomic positions[25]. However, this positional disorder of the rare earth atom has been observed in a variety of related systems, including LuCuGaO$_4$, LuCoGaO$_4$, YbCuGaO$_4$, LuCuFeO$_4$, LuZnFeO$_4$[8], and YbMgGaO$_4$[21], suggesting that TmMgGaO$_4$ behaves similarly. A powder Rietveld refinement was also performed using a model where the Tm^{3+} ion sits directly on the high symmetry site (i.e., it is not displaced). This refinement resulted in a poorer fit. A comparison of the resulting values for both refinements can be seen in Table 2. We

also performed single-crystal XRD refinement of the structure to probe the Tm disorder (see Supplementary Information). The statistic positional disorder of the Tm positions can also be described by a model wherein the Tm atom sits directly on the high-symmetric Wyckoff site *3a* [0 0 0] site but has a very large anisotropic displacement parameter along the *c*-axis. The results of this refinement can be seen in the supplementary information, along with a map of the measured atomic scattering density showing the distribution of thulium positions in a section of the unit cell, derived from the observed structure factors, F_{obs}. Large dynamic motion of the Tm atom around the high symmetry site is not physically realistic and therefore this model cannot be considered correct.
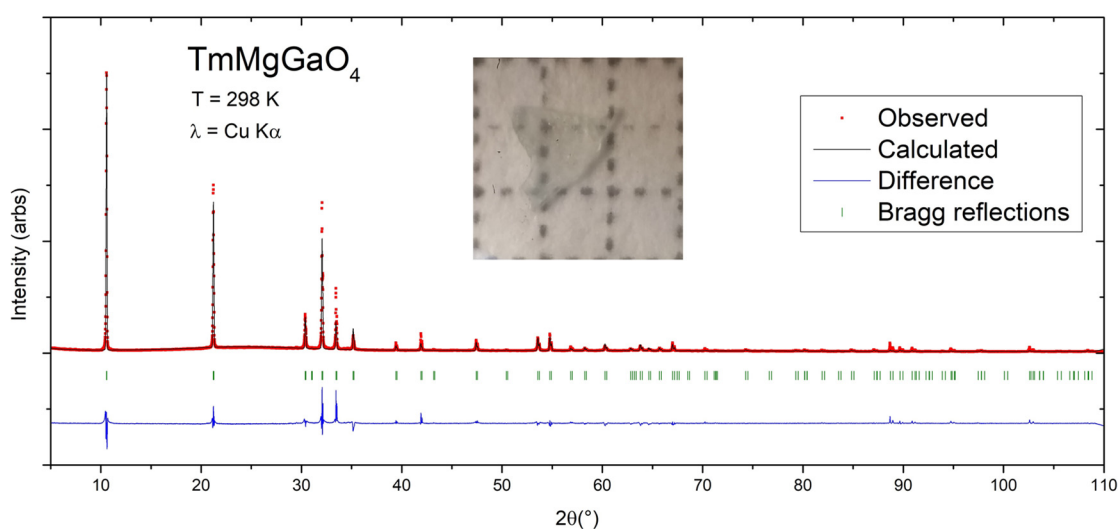

Figure 1. Powder Rietveld refinement of TmMgGaO₄. Inset: A small, colorless transparent single crystal of TmMgGaO₄ on a 1-mm grid.

Table 1. Refined crystal structure of TmMgGaO$_4$ at ambient temperature, space group *R-3m* (no. 166), unit cell parameters a = 3.4195(3) Å and c = 25.1231(12) Å, from the ambient temperature powder X-ray diffraction data. R_f factor = 17.1, R_p = 10.1, R_{wp} = 14.7, χ^2 = 13.7.

Atom	Wyckoff site	x	y	z	Occ.
Tm	*6c*	0	0	0.0078(2)	0.5
Mg	*6c*	0	0	0.2147(2)	0.5
Ga	*6c*	0	0	0.2147(2)	0.5
O1	*6c*	0	0	0.2836(4)	1
O2	*6c*	0	0	0.1368(4)	1

Table 2. Comparison of selected values resulting from Rietveld powder refinements of two models for TmMgGaO$_4$. In Model 1, the Tm^{3+} atom is displaced from the high-symmetry site. In Model 2, the Tm^{3+} atom sits directly on the high symmetry site (*3a*).

|	Model 1		Model 2	
Atom	z	Biso	z	Biso
Tm^{3+}	0.0078(2)	1.543(122)	0.0000	3.206(129)
Mg^{2+}/Ga^{3+}	0.2147(2)	1.082(141)	0.2157(1)	1.358(163)
O1	0.2836(4)	1.729(377)	0.2820(4)	4.494(499)
O2	0.1368(4)	4.262(572)	0.1391(3)	2.992(535)
Rietveld R-Factor				
R_f	17.1		18.1	
R_p	10.1		10.5	
R_{wp}	14.7		15.3	
χ^2	13.7		14.9	
Bond				
Tm^{3+} — O1 (x6) (Å)	2.238(5)		2.358(6)	
Mg^{2+}/Ga^{3+} — O1 (Å)	1.730(10)		1.665(12)	
Mg^{2+}/Ga^{3+} — O2 (x3) (Å)	2.026(2)		2.047(2)	
Mg^{2+}/Ga^{3+} — O2 (Å)	1.958(10)		1.932(9)	
O1 — O1 (x6) (Å)	3.4195(2)		3.4195(2)	
O1 — O1 (x3) (Å)	3.185(10)		3.248(12)	
O1 — O2 (x3) (Å)	2.946(10)		2.961(10)	
O2 — O2 (x3) (Å)	2.480(8)		2.410(7)	
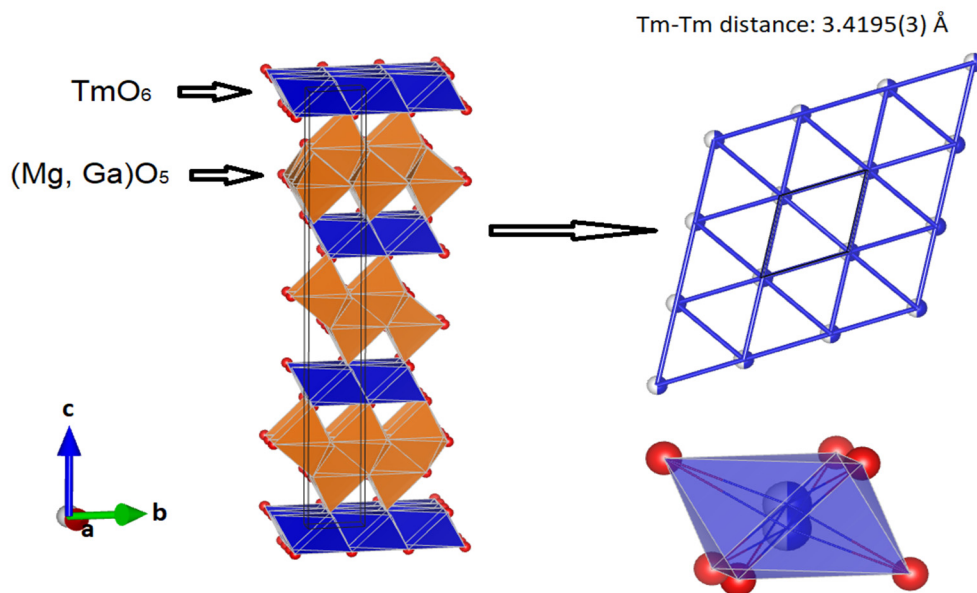
Figure 2. The crystal structure of $TmMgGaO_4$ showing the coordination polyhedra. TmO_6 octahedra are blue, GaO_5 or MgO_5 triangular bipyramids are orange. On the right is the triangular magnetic lattice formed by the Tm layers, as viewed along the *c*-axis. In the bottom right is a closer look at the distorted nature of the TmO_6 octahedra.

Magnetism

The temperature-dependent magnetic susceptibility of a powder sample of $TmMgGaO_4$ (sample produced by grinding a collection of small single crystals) is shown in Figure 3. The susceptibility was fit to the Curie-Weiss law $\chi - \chi_0 = C / (T - \theta_W)$, where χ is the magnetic susceptibility, χ_0 is a temperature-independent contribution, C is the Curie constant, and θ_W is the Weiss temperature. The inverse susceptibility, $1/(\chi - \chi_0)$, was found to be almost linear for a χ_0 value of 0.0010 emu mol^{-1}. The χ_0 value for the polycrystalline sample is consistent with the single crystal susceptibility obtained for fields in the plane of the triangular lattice, as described below. The inverse susceptibility was fit at high and low temperature. At high temperature (150 K – 290 K), C was found to be 7.26 and θ_W was found to be -25.6 K. The effective magnetic moment per ion, μ_{eff}, was

determined by the relationship $\mu_{eff} = \sqrt{8C}$, yielding a moment of 7.62 μ_B/Tm, in good agreement with the ideal value for a free Tm^{3+} ion, 7.57 μ_B. At low temperatures, a linear fit yielded values of C = 6.68, θ_W = -19.7, and an effective magnetic moment of 7.31 μ_B/Tm. The negative Weiss temperatures determined by these fits suggest that $TmMgGaO_4$ has dominantly antiferromagnetic coupling, but no magnetic ordering is observed down to 1.8 K. At the lowest temperatures studied here (1.8-10 K) there is a deviation from the paramagnetic behavior predicted by the higher temperature Curie Weiss fits (Figure 3, inset). $TmMgGaO_4$ therefore exhibits a frustration index f (θ_W /T_M) of 10 or more, suggesting that it is a strongly frustrated magnet[4].
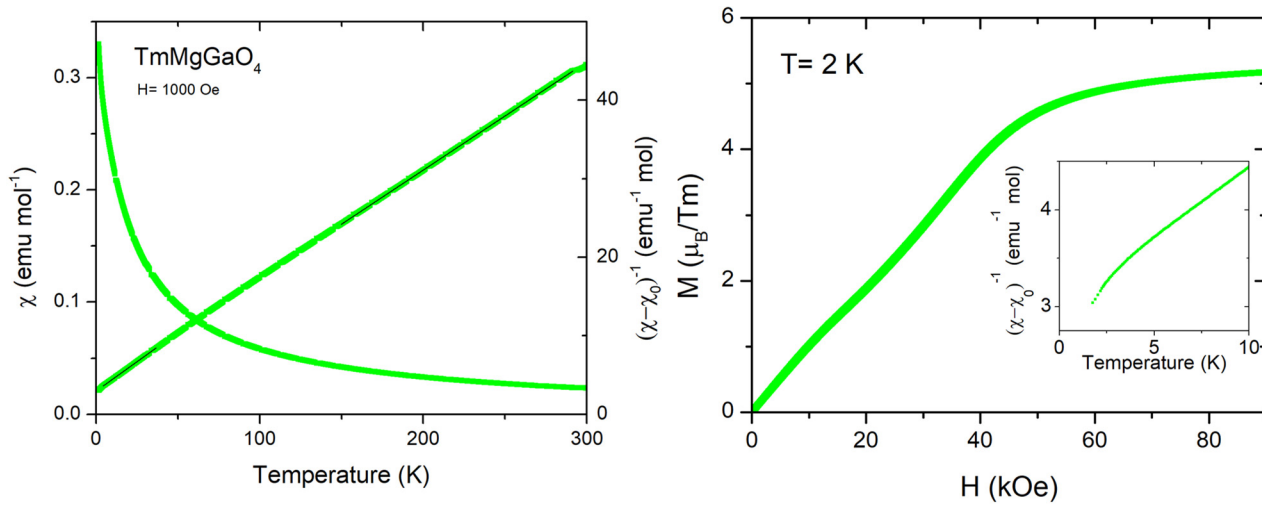

Figure 3. Left panel: The temperature-dependent DC magnetic susceptibility and reciprocal susceptibility of a polycrystalline powder of $TmMgGaO_4$ in an applied field of 1000 Oe. Curie-Weiss fits are shown in black. Right panel: The field-dependent magnetization at 2 K. Inset: Magnified view of the low-temperature region of the inverse susceptibility.

A magnetization vs. applied field measurement was taken on the same powder sample at 2 K.

The material exhibited a nonlinear magnetization response with an apparent saturation of approximately 5 μ_B/Tm at applied fields of 8 Tesla. Repeating this measurement on a small single crystal of TmMgGaO$_4$ perpendicular to the triangular plane (i.e. parallel to the c-axis) resulted in a much higher saturation magnetization, of approximately 7 μ_B/Tm (Figure 4). The presence of this saturation, in spite of no visible evidence of magnetic ordering at this temperature, is also observed in the closely-related materials YbMgGaO$_4$[18,21] and YbZnGaO$_4$[27]. **In other frustrated rare-earth systems, the saturation of magnetization with applied field has been attributed to a magnetic state that is stable at intermediate fields, involving magnetic-field-induced spin alignment along one or more preferred directions in the crystal structure[6,28]. The same type of effect may be operating in the current system**. Both the powder and single-crystal magnetizations demonstrate a slope anomaly with an onset field of approximately $\mu_0 H \sim 2$ Tesla. The origin of this anomaly is currently unknown, but its appearance is reminiscent of metamagnetism and its presence is consistent across all samples. In contrast, magnetization vs. applied field measurements conducted parallel to the triangular planes (i.e. perpendicular to c) yielded very different results: a much smaller magnetization with a very slight curvature and no apparent saturation. From this it can be safely concluded that TmMgGaO$_4$ has a high degree of magnetic anisotropy, which we attribute to crystal electric field (CEF) effects originating from its layered crystal structure and distorted TmO$_6$ octahedra. This distortion of the octahedra results from the previously-described off-site nature of the central Tm atoms, which has been attributed to local distortions caused by disorder on the Mg/Ga sites. We note that strong CEF effects have been found in the isostructural compound YbMgGaO$_4$[20], lending credence to our hypothesis concerning the origin of the magnetic anisotropy.
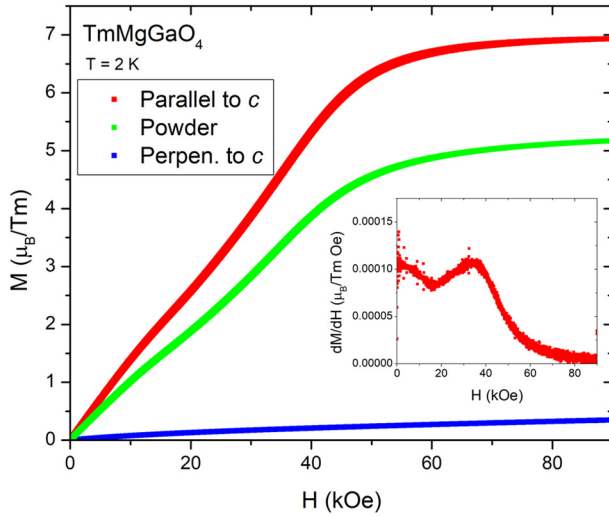
Figure 4. Magnetization vs applied field measurements on a single crystal of TmMgGaO4 parallel to the c-axis, perpendicular to the *c*-axis, and on a powder sample of the same material. Inset: Derivative of magnetization parallel to the *c*-axis with respect to applied field.

In order to observe this anisotropy more clearly, magnetization vs temperature measurements were taken on a single crystal (pictured in Figure 1), both parallel and perpendicular to the triangular layers. As can be seen in Figure 5, the anisotropy is clearly displayed in this measurement as well. Measurements parallel to the perpendicular to the triangular planes (i.e. along the *c*-axis) yielded a similar curve to the powder sample, but much larger values of molar magnetic susceptibility. Measurements parallel to the planes show a much weaker signal, with a broad region spanning from 50 K to 300 K that appears to be nearly temperature-independent. The purple curve in Figure 5 is a weighted average of the temperature-dependent susceptibilities of the single crystal (1/3 of the value parallel to the *c*-axis plus 2/3 of the value perpendicular to the c-axis). This calculated value overlaps almost exactly with the measured susceptibility of the powder. In the right panel of Figure 5, the

inverse is shown of all four susceptibilities. The weighted average of the anisotropic susceptibilities in this case is more linear than the unmodified inverse susceptibility of the powder, but when the term χ_0 (which we attribute to the container for the powder sample) is applied to the powder measurement, the two once again overlap almost exactly. The observation that the magnetic moment as measured in a polycrystalline powder is effectively a simple average of the moments along the spatial directions is consistent with the hypothesis that this anisotropy arises as a result of CEF effects within the crystal lattice[29]. This may also explain the anisotropy at high temperatures, as CEF effects sometimes result in large paramagnetic anisotropies[29].
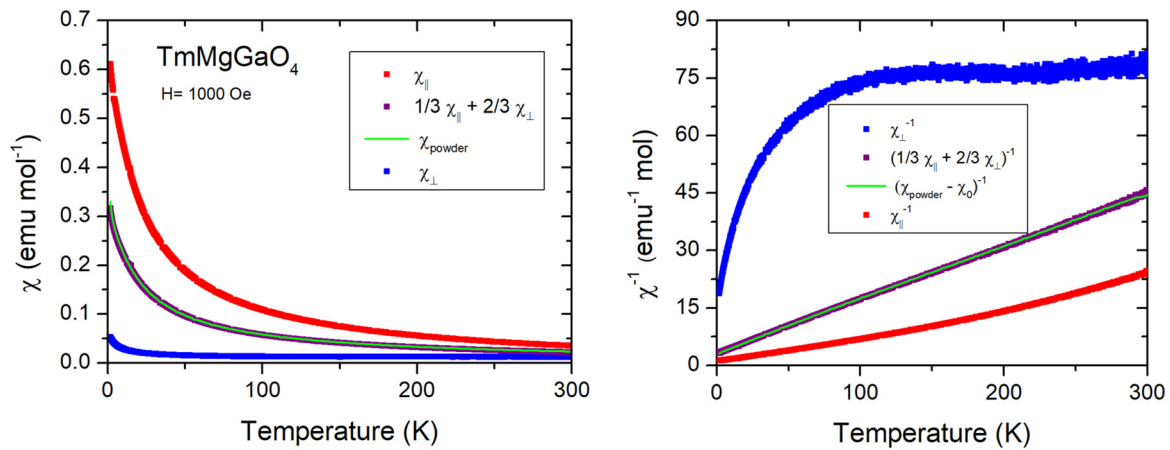

Figure 5. Left panel: The temperature-dependent DC susceptibility of a single crystal of $TmMgGaO_4$ as measured parallel to the *c*-axis (red) and perpendicular to the *c*-axis (blue). In purple is a weighted average of the directional susceptibilities. The measured susceptibility of the polycrystalline powder is superimposed in green. Right panel: The reciprocal susceptibilities of the single crystal and polycrystalline powder.

Conclusion

Single crystals of $TmMgGaO_4$ have been synthesized in an optical floating zone furnace, and the structure has been refined. The resulting values for lattice parameters and atomic positions are in good agreement with previously published results for this and other isostructural compounds. Magnetization measurements were performed, finding the material to display dominantly antiferromagnetic interactions, with no ordering above 1.8 K. Thus the magnetic characterization suggests a magnetic frustration index of 10 or more. Magnetization measurements on a single crystal show that the magnetic properties are highly anisotropic, and suggest that this anisotropy may arise from CEF effects. Further characterization of the low temperature properties of this material is warranted; the uncommon interplay of an isolated, geometrically-frustrated magnetic 2D lattice, and the subtle structural distortions induced on the magnetic interactions due to the off-plane disorder of non-magnetic ions may give rise to unusual electronic or magnetic ground states, and similar to the disordered transition metal pyrochlores, may provide interesting system for testing the effect of disorder in geometrically frustrated magnets[30-35]. Further efforts to grow larger high-quality single crystals for complimentary measurement purposes, such as neutron scattering, may also be of interest.

Acknowledgments

References

1. Lacroix, C., Mendels, P., Mila, F., *Introduction to Frustrated Magnetism* (Springer-Verlag Berlin Heidelberg, 2011).

2. Diep, H. T. *et al.*, *Frustrated Spin Systems* (World Scientific Publishing Co., Singapore, 2004).

3. Sadoc, J. F., Mosseri, R., *Geometrical Frustration* (Cambridge University Press, Cambridge, 1999).

4. Ramirez, A. P., *Annu. Rev. Mater. Sci.*, **24**, 453-480 (1994).

5. Moessner, R., Ramirez, A. P., *Phys. Today*, **59** (2), 24 (2006).

6. Gardner, J. A., Gingras, M. J. P., Greedan, J. E., *Rev. Mod. Phys.*, **82** (53), (2010).

7. Balents, L., *Nature*, **464** (2010).

8. Cava, R.J., Ramirez, A.P., Huang, Q., Krajewski, J.J. *J. Solid State Chem.* **140** (2), 337-344 (1998).

9. Fritsch, K., Ross, K. A., Granroth, G. E., Ehlers, G., Noad, H. M. L., Dabkowska, H. A., Gaulin, B. D., *Phys. Rev. B*, **96**, 094414 (2017).

10. Dabkowska, H. A., Dabkowska, A., Luke, G. M., Gaulin, B. D., *J. Crys. Growth*, **234** (2-3), 411-414 (2002).

11. Iida, J., Tanaka, M., Nakagawa, Y., *J. Phys. Soc. Jpn.*, **59**, 4443-4448 (1990).

12. Hearmon, A. J., Prabhakaran, D., Nowell, H., Fabrizi, F., Gutmann, M. J., Radaelli, P. G., *Phys. Rev. B*, **85**, 014115 (2012).

13. Zhang, Y., Yang, H. X., Guo, Y. Q., Ma, C., Tian, H. F., Luo, J. L., Li, J. Q., *Phys. Rev. B*, **76**, 184105 (2007).

14. Liu, Y., Zou, T., Wang, F., Zhang, X., Cheng, Z., Sun, Y. *Physica B. Cond. Mat.*, **405** (16), 3391-3394 (2010).

15. Ikeda, N. *J. of Phys. Cond. Mat.* **20** (43), (2008).

16. Zhang, Y., Yang, H. X., Ma, C., Tian, H. F., Li, J. Q. *Phys. Rev. Lett.,* **98**, 247602 (2007).

17. Kato, K., Kawada, I., Kimizuka, N., Katsura, T., *Zeit. Für Krist.,* **141**, 314-320 (1975).

18. Li, Y., Chen, G., Tong, W., Pi, L., Liu, J., Yang, Z., Wang, X., Zhang, Q. *Phys. Rev. Lett.* **115**, 167203 (2015).

19. Paddison, J. A. M., Daum, M., Dun, Z. L., Ehlers, G., Liu, Y., Stone, M. B., Zhou, H. D., Mourigal, M. *Nature Physics* **13**, 177-122 (2017).

20. Li, Y., Adroja, D., Bewley, R., Voneshen, D., Tsirlin, A., Gegenwart, P., Zhang, Q. *Phys. Rev. Lett.* **118**, 107202 (2017).

21. Li, Y., Liao, H., Zhang, Z., Li, S., Jin, F., Ling, L., Zhang, L., Zou, Y., Pi, L., Yang, Z., Wang, J., Wu, Z., Zhang, Q. *Sci. Reports,* **5**, 16419 (2015).

22. Shen, Y., Li, Y.-D., Wo, H., Li, Y., Shen, S., Pan, B., Wang, Q., Walker, H. C., Steffens, P., Boehm, M., Hao, Y., Quintero-Castro, D. L., Harriger, L. W., Frontzek, M. D., Hao, L., Meng, S., Chang, Q., Chen, G., Zhao, J., *Nature*, **540**, 559-562 (2016).

23. Zhu, Z., Maksimov, P. A., White, S. R., Chernyshev, A. L., *Phys. Rev. Let.*, **119**, 157201 (2017).

24. Kimizuka N., and Takayama, E. *J. Solid State Chem.* **41**, 166-173 (1982).

25. Beznosikov, B. V. and Aleksandrov, K. S. *Krasnoyarsk.* Pre-print (2006).

26. Kimizuka, N., and Mohri, T. *J. Solid State Chem.* **60** (3), 382-384 (1985).

27. Ma, Z., Wang, J., Dong, Z., Zhang, J., Li, S., Zheng, S., Yu., Y., Wang, W., Che, L., Ran, K., Bao, S., Cai, Z., Cermak, P., Schneidewind, A., Yano, S., Gardner, J. S., Lu, X., Yu, S., Liu, J., Li, S., Li, J., Wen, J. *Phys. Rev. Lett.*, **120**, 087201 (2018).

28. **Rule, K. C., Ruff, J. P. C., Gaulin, B. D., Dunsinger, S. R., Gardner, J. S., Clancy, J. P., Lewis, M. J., Dabkowska, H. A., Mirebau, I., Manuel, P., Qiu, Y., Copley, J. R. D.,** ***Phys. Rev. Lett.,*** **96, 177201 (2006).**

29. Dunlap, B. D., *J. Mag. and Mag. Mat.*, **37**, 211-214 (1983).

30. Sanders, M. B., Krizan, J. W., Plumb, K. W., McQueen, T. M., Cava, R. J., *J. Phys. Condes Matter*, **29**, 045801 (2017).

31. Krizan, J. W., Cava, R. J., *Phys. Rev. B*, **92**, 014406 (2015).

32. Krizan, J. W., Cava R. J., *Phys. Rev. B*, **89**, 214401 (2014).

33. Saunders, T. E., Chalker, J. T., *Phys. Rev. Lett.*, **98**, 157201 (2007).

34. Andreanov, A., Chalker, J. T., Saunders, T. E., Sherrington, D., *Phys. Rev. B*, **81**, 014406 (2010).

35. Silverstein, H. J., Fritsch, K., Flicker, F., Hallas, A. M., Gardner, J. S., Qiu, Y., Ehlers, G., Savici, A. T., Yamani, Z., Ross, K. A., Gaulin, B. D., Gingras, M. J. P., Paddison, J. A. M., Foyetsova, K., Valenti, R., Hawthorne, F., Wiebe, C. R., Zhou, H. D., *Phys. Rev. B*, **89**, 054433 (2014).